2018

In vivo monitoring of intracellular Ca2+ dynamics in the pancreatic β-cells of zebrafish embryos

Reka Lorincz

Christopher H. Emfinger

Andrea Walcher

Michael Giolai

Claudia Krautgasser

See next page for additional authors

Authors

Reka Lorincz, Christopher H. Emfinger, Andrea Walcher, Michael Giolai, Claudia Krautgasser, Maria S. Remedi, Colin G. Nichols, and Dirk Meyer

In vivo monitoring of intracellular Ca^{2+} dynamics in the pancreatic β-cells of zebrafish embryos

Reka Lorincz, Christopher H. Emfinger, Andrea Walcher, Michael Giolai, Claudia Krautgasser, Maria S. Remedi, Colin G. Nichols & Dirk Meyer

Taylor & Francis
Taylor & Francis Group

RESEARCH PAPER

🔓 OPEN ACCESS ⟳ Check for updates

In vivo monitoring of intracellular Ca^{2+} dynamics in the pancreatic β-cells of zebrafish embryos

Reka Lorincz [a], Christopher H. Emfinger [b,c,d], Andrea Walcher [a], Michael Giolai [a], Claudia Krautgasser[a], Maria S. Remedi [b,d], Colin G. Nichols [b,c], and Dirk Meyer [a]

aInstitute of Molecular Biology/CMBI, University of Innsbruck, Innsbruck, Austria; bDepartment of Cell Biology and Physiology, Washington University School of Medicine, St. Louis, MO, USA; cCenter for the Investigation of Membrane Excitability Diseases (CIMED), Washington University School of Medicine, St. Louis, MO, USA; dDepartment of Medicine, Washington University School of Medicine, St. Louis, MO, USA

ABSTRACT

Assessing the response of pancreatic islet cells to glucose stimulation is important for understanding β-cell function. Zebrafish are a promising model for studies of metabolism in general, including stimulus-secretion coupling in the pancreas. We used transgenic zebrafish embryos expressing a genetically-encoded Ca^{2+} sensor in pancreatic β-cells to monitor a key step in glucose induced insulin secretion; the elevations of intracellular [Ca^{2+}]$_i$. *In vivo* and *ex vivo* analyses of [Ca^{2+}]$_i$ demonstrate that β-cell responsiveness to glucose is well established in late embryogenesis and that embryonic β-cells also respond to free fatty acid and amino acid challenges. *In vivo* imaging of whole embryos further shows that indirect glucose administration, for example by yolk injection, results in a slow and asynchronous induction of β-cell [Ca^{2+}]$_i$ responses, while intravenous glucose injections cause immediate and islet-wide synchronized [Ca^{2+}]$_i$ fluctuations. Finally, we demonstrate that embryos with disrupted mutation of the Ca$_V$1.2 channel gene *cacna1c* are hyperglycemic and that this phenotype is associated with glucose-independent [Ca^{2+}]$_i$ fluctuation in β-cells. The data reveal a novel central role of *cacna1c* in β-cell specific stimulus-secretion coupling in zebrafish and demonstrate that the novel approach we propose – to monitor the [Ca^{2+}]$_i$ dynamics in embryonic β-cells *in vivo* – will help to expand the understanding of β-cell physiological functions in healthy and diseased states.

Introduction

Assessing the response of pancreatic islet cells to glucose stimulation is important for understanding β-cell function in healthy and diseased states. Until now, pancreatic β-cell physiology has been analyzed mainly in isolated cell and islet systems.[1–5] Importantly, β-cells under these conditions likely exhibit different physiology when compared to cells in their natural *in vivo* environment. A key step in mammalian glucose-stimulated insulin secretion is the elevation of intracellular [Ca^{2+}]$_i$. Non-invasive *in vivo* imaging of [Ca^{2+}]$_i$ has recently been facilitated by transplantation of pancreatic islets into the anterior chamber of the eye or the kidney capsule of mice. Such real-time monitoring facilitates the study of islet physiology and vascularization longitudinally, and enables *in vivo* screening of novel drugs and treatments.[6]

Ultimately, however, it is desirable to incorporate *in vivo* imaging of native intracellular [Ca^{2+}]$_i$ without interfering with the complex paracrine signalling networks regulating islet activity in native tissue (for a review, see ref.[7]) Here we tested transgenic zebrafish embryos expressing a genetically encoded Ca^{2+} sensor in their β-cells as a potential model for corresponding non-invasive *in vivo* applications. Non-mammalian vertebrates such as zebrafish (*Danio rerio*) have become relevant alternative organisms to study diabetes and other metabolic diseases,[8] due to ease of genetic manipulation, high reproduction rates, and ready access for *in vivo* imaging due to larval transparency. Importantly, pancreata in mammals and in zebrafish have conserved physiological endocrine and exocrine function, similar cellular architecture, and conserved expression and function of

---

most developmental genes.[9] Accordingly, the zebrafish has proven highly productive for studies of pancreas development,[10–12] and regeneration.[13,14] In mammals as well as in zebrafish the pancreas develops from the endodermal germ layer and later compromises endocrine and exocrine tissue.[15] Within one day of development, the zebrafish embryo forms a single 'primary' pancreatic islet with ~60–70 mono-hormonal α-, β-, δ-, ε-cells. As development proceeds, the primary islet increases in size and additional secondary islets are formed, to adopt to growth-related requirements.

Glucose metabolism in zebrafish is also very similar to mammalian glucose metabolism, and overfed zebrafish displays obesity-related diabetes phenotypes including impaired glucose tolerance and increased insulin production.[16] The molecular basis of glucose detection is well understood in mammalian pancreatic β-cells (for a review, see ref.[17] and.[18]) Glucose is taken up by the facilitative glucose transporter (GLUT) GLUT2/SLC2A2, and is metabolized through glycolysis and oxidative phosphorylation, thereby generating adenosine triphosphate (ATP) and increasing the ATP/ADP ratio.[11,19] The altered [ATP/ADP] ratio in the β-cell then leads to the closure of ATP-sensitive K^+-channels (K_{ATP}-channels), depolarization of the membrane, and consequent opening of voltage-dependent calcium channels (VDCCs).[20] The influx of Ca^{2+} then triggers release of insulin from secretory granules.[21] Orthologues of all major genes (GLUT, K_{ATP}-channels and VDCCs) involved in mammalian glucose sensing and insulin secretion are also expressed in zebrafish, and show functional similarities.[22–25] Studies suggest that glucose uptake in zebrafish, similar to mammals, occurs through GLUT transporters, with GLUT2 expression found in the endocrine pancreas of zebrafish larvae.[26,27] Furthermore, we and others recently demonstrated that zebrafish islet β-cells express functional K_{ATP} channels with conserved structure and metabolic sensitivity to their mammalian counterparts, supporting the use of zebrafish as a model animal in islet glucose sensing and diabetes research.[28,29]

Excitability of β-cells has been investigated by multiple strategies including monitoring of the membrane potential by electrical recordings, and using Ca^{2+}-sensitive dyes.[30–32] More recently, genetically encoded Ca^{2+} indicators have been introduced as tools for non-invasive approaches to study excitable cells such as β-cells. The analysis of Ca^{2+} transients in corresponding models systems will help in understanding underlying causes of β-cell dysfunction (for example in the context of diabetes risk factors.[33,34]) In vivo imaging of $[Ca^{2+}]_i$ dynamics in transplanted (intraocular) mouse pancreatic islets showed reduction at a prediabetic stage, suggesting the potential of $[Ca^{2+}]_i$ as a functional marker to evaluate β-cells in vivo in diseased states.[35] Nevertheless, the low litter numbers, complicated methodologies, high costs, and large experiment variability limit the use of mammalian species for such studies. Since genetic manipulation is easy and inexpensive in transparent zebrafish larvae, large-scale drug and genetic screens as well as fluorescent imaging applications for studying β-cell physiology in living animals are feasible.[36–38] Monitoring of the glucose-stimulated Ca^{2+} influx in isolated juvenile and larvae zebrafish islets has been previously described.[39] We recently generated a transgenic line expressing the genetically encoded Ca^{2+}-sensor GCaMP6s, and in this study we have established protocols for in vivo monitoring of $[Ca^{2+}]_i$ dynamics in late embryonic animals. We found that β-cells in larvae show rare baseline spontaneous activities, but after intravenous injections of glucose, virtually all β-cells showed very rapid elevations in GCaMP6s fluorescence.

Additionally, we have used the GCaMP6s reporter to assess β-cell associated function of VDCCs. β-cell specific $Ca_V1.2^{-/-}$ mice exhibit mild basal hyperglycemia, impaired glucose tolerance and lack of first-phase insulin secretion,[40,41] but this important role in mammalian glucose-induced insulin secretion has not been assessed in zebrafish.[40–43]

Results

Zebrafish β-cell $[Ca^{2+}]_i$ responses depend on the route of glucose administration in vivo

To enable *in vivo* studies of β-cell $[Ca^{2+}]_i$ in zebrafish larva, we generated a transgenic line expressing a genetically encoded membrane-tagged Ca^{2+}-sensor together with a Histone-

tagged RFP, both under control of the insulin promoter (Tg[ins:lynGCaMP6s; ins:H2B-RFP], referred to hereafter as ins:lynGCaMP6s; Figure 1(A,B)). The combined expression of lynGCaMP6s and H2B-RFP in β-cells enabled rapid β-cell identification and measurements of Ca^{2+} responses in selected β-cell areas. We further established protocols for determining β-cell specific Ca^{2+} changes either in the living embryo (Figure 1(C)) or in isolated islets (Figure 1(D)). In the first set of experiments, we recorded β-cell responses to different routes of glucose administration. To simulate physiologically relevant feeding-related gradual and continued increase of blood glucose level, we tested injections of glucose into the yolk, the
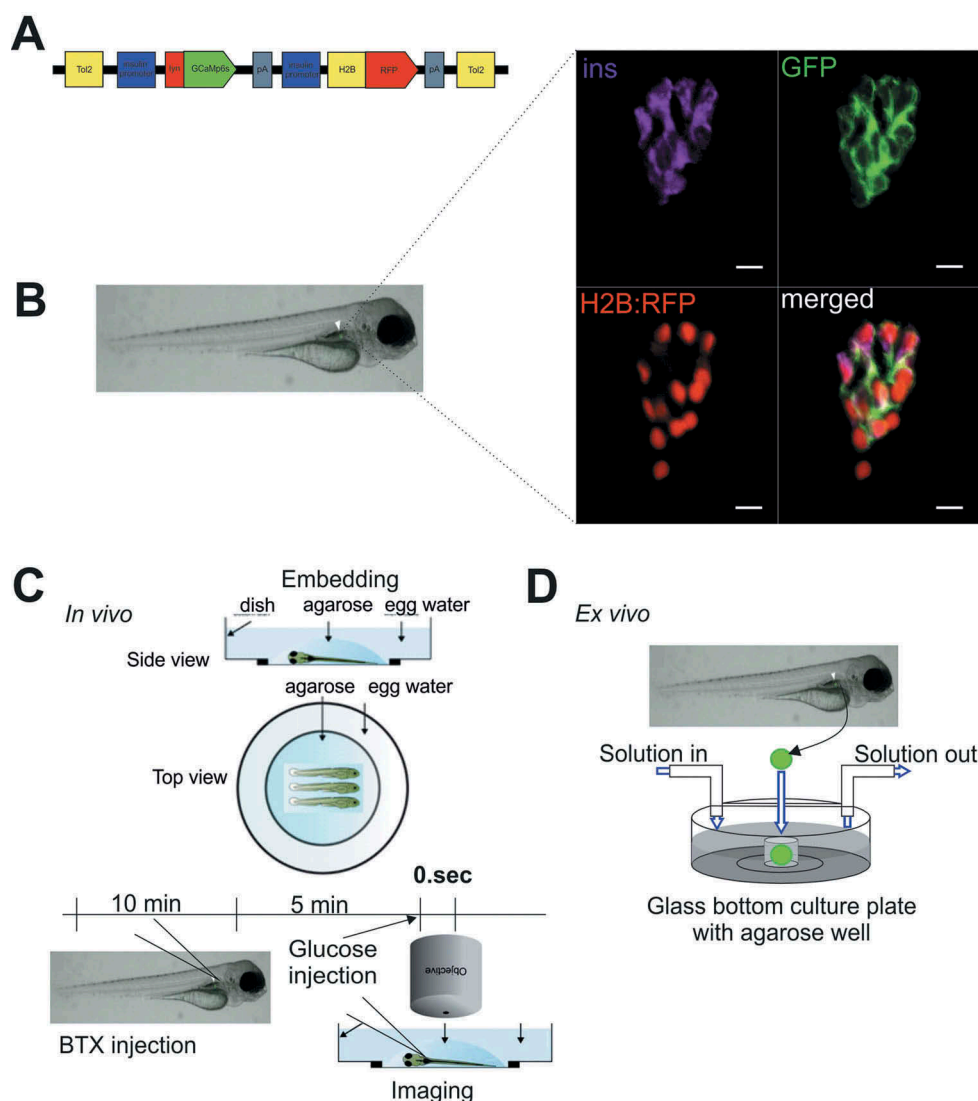

Figure 1. Specific expression of GCaMP6s sensor in pancreatic β-cells enables the study of Ca2+ fluxes in live zebrafish.

(A) Illustration of the construct used to generate Tg[ins:lynGCaMP6s ins:H2BtagRFP] (ins:lynGCaMP6s). The GCaMP6s sensor was linked N-terminal with a lyn membrane tag. The additional ins:H2BtagRFP sequence was added to the construct to ease the screening of transgenic embryos and to identify the β-cells due to the nuclear specific H2BtagRFP signal. **(B)** Antibody staining on 5 days post fertilization (dpf) ins:lynGCaMP6s embryos detecting >95% overlapping of endogenous insulin and GCaMP6s (using polyconal GFP antibody) and >80% overlapping of H2B:RFP and GCaMP6s (n = 12 larvae, 20 β-cells per larva were analysed). **(C)** Schematic outline of intravenous glucose injection of zebrafish larvae. Using α-bungarotoxin (BTX) protein injection, the zebrafish larvae are paralyzed. After 10–15 min, the larvae are embedded in low melt agarose. Using a micromanipulator assembled to the microscope, glucose (in combination with Rhodamine B isothiocyanate-Dextran) is injected to the dorsal aorta of the embryo while the imaging is running. **(D)** Schematic outline of perfusion system on extracted pancreatic islet of zebrafish embryos. Islets from ins:lynGCaMP6s fish are isolated and placed into glass-bottomed culture plates with agarose gel wells containing islet media for Ca^{2+} imaging as solutions are changed. Scale bar = 10 μm

pericardium or the hindbrain ventricle. In all approaches, the glucose injection induced Ca^{2+} fluctuation in β-cells (Sup. Fig. 1D–F), but the responses were very variable, with delays between injection and response ranging from seconds to minutes and the number of

responsive cells varying from 5–30% (Sup. Fig. 1A–C). In contrast, intravenous injection of D-glucose (~10–20 mM final concentration) in wild-type 5 dpf larvae evoked rapid and robust elevations in the GCaMP6s fluorescence in almost all labelled cells (Figure 2(A), blue
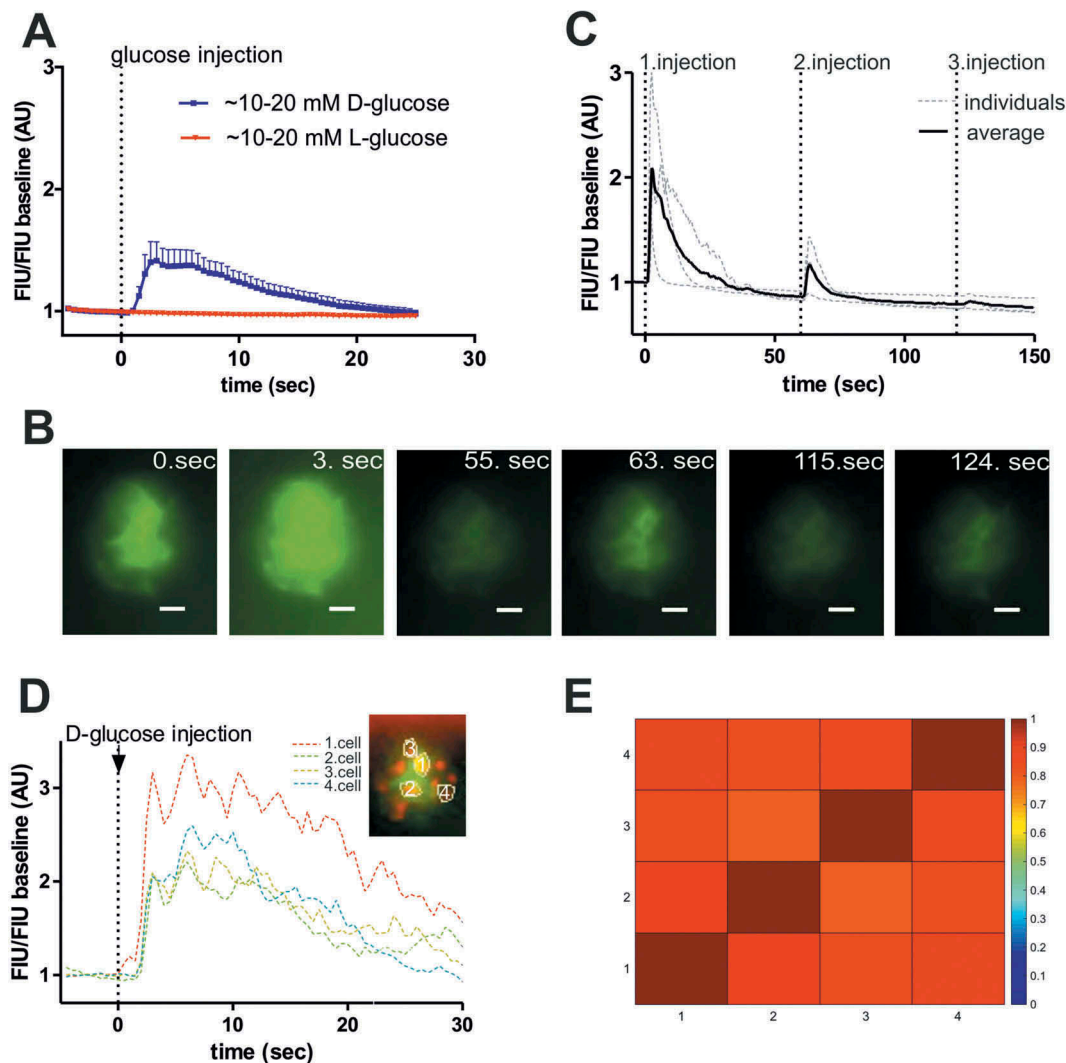

Figure 2. Zebrafish β-cells show rapid glucose response in vivo.

(A) *In vivo* experiments in larva revealed rapid fluorescence signal alteration (peak within 5 sec) in response to intravenous injection of >10 mM D-glucose (blue line) (5 dpf) (n = 8 larvae). To confirm that the response is due to D-glucose metabolism, L-glucose (red line) using same concentration (>10 mM) was also injected and showed no response (n = 5 larvae). **(B)** Fluorescence image series of the islet showing β-cell specific GCaMP6 signal at the indicated time-points (sec) after intravenous injection of D-glucose (>10 mM final concentration) in 5 dpf larva. Scale bar = 10 μm **(C)** Quantitative GCaMP6 signal intensity in the larvae shown in **(B)**, and two other individual larvae (gray dotted lines), showing calcium influx after sequential glucose injections (1.injection: >10 mM, 2. Injection: >20 mM, 3. Injection: >30 mM estimated final concentration). FIU intensities for the whole islet were determined using Image-J and normalized to the FIU baseline (intensity measured in the first time point). **(D)** Representative fluorescence traces of manually selected β-cell areas (n = 4, based on red RFP expression as indicated) in a 5 dpf old zebrafish larva, normalized to initial fluorescence intensity, while 1–2 nl of 0.5 M D-glucose (>10 mM final concentration) was intravenously injected *in vivo* (at dotted black line). After glucose injection β-cell areas show oscillation. **(E)** Cross-correlation matrix (determined by PeakCaller, MATLAB) of the 4, in (D) indicated, β-cell areas after intravenous glucose injection. The panel represent one islet with 4–4 cell comparison. Colour map key is given to the right of the panel. Further examples are shown in Sup. Fig. 2B. FIU = Fluorescence Intensity Units (AU, Arbitrary Units).

line). Sequential intravenous glucose injections resulted in repeated similar rapid responses, but the normalized Fluorescence Intensity Unit (FIU) peaks decreased after the second and third injection (Figure 2(B),(C)). Control injections with the same concentration of L-glucose caused no GCaMP6s signals (Figure 2(A), red line), confirming that the response is due to glucose metabolism, rather than osmotic stress or other potential injection artefacts. In intravenously D-glucose-injected embryos, the fluorescence increased almost immediately after injection, and reached its peak within 5 seconds, followed by oscillations across the islets (5 ± 1 peaks/minute; Figure 2(D), Sup.Video 1 and 2). Correlation analyses revealed that glucose-induced responses are synchronized across the islet when the glucose is injected intravenously (Figure 2(E) and Sup. Fig. 2B), which was not the case for yolk injection (Sup. Fig. 2C), indicating that the *in vivo* responsiveness of zebrafish β-cells to glucose depends on the route of glucose administration.

Zebrafish islets are glucose responsive in early developmental stages

We next assessed whether the glucose-responsiveness of β-cells observed in 5 dpf larvae is also seen at earlier developmental stages. Studies in rodents have established that islet maturity and function vary during development, with glucose responsiveness occurring in later stages, particularly near the weaning transition.[44] Previous studies showed that insulin-dependent glucose homeostasis in zebrafish starts at 3 dpf.[45] Normalized FIU intensities showed similar glucose-induced $[Ca^{2+}]_i$ dynamics over time (Figure 3(a)), and quantification of the GCaMP6s signal revealed significantly higher peak FIU intensities after glucose injection compared to baseline (before glucose), but no significant differences between developmental stages (3, 4 and 5 dpf) (Figure 3(b)). In addition, little or no spontaneous responses were observed in unstimulated larvae at 3–5 dpf (Figure 3(c,d)). This shows that the embryonic onset of insulin-dependent glucose homeostasis correlates with the requirement for glucose-sensing mechanisms after 3 dpf.

Zebrafish islets are uncoupled ex vivo

To assess the concentration-dependence of glucose and other nutrients on β-cell excitation, we performed perfusion studies with isolated pancreatic islets (*ex vivo*) from 5 dpf old zebrafish larvae (Figure 1(D)). Isolated larval islets were first incubated in 2 mM glucose solution, then stimulated with 20 mM glucose solution and at the end of the recording, 30 mM KCl solution was applied to confirm excitability. In these experiments, higher resolution imaging by spinning disc microscopy enabled single cell analysis of the isolated islets. Consistent with the *in vivo* data, 20 mM glucose increased GCaMP6s FIU/FIU baseline intensity (Figure 4(A,B)), almost all β-cells (83% ± 24%, Figure 4(C)) responded to the glucose stimulus, and the induced $[Ca^{2+}]_i$ oscillated with similar frequencies (5 ± 1 and 6 ± 1 peaks/minute, respectively, Figure 4(D)). However, in contrast to what was observed after intravenous glucose injection, *ex vivo* β-cell responses were out of phase (correlation analyses shown Figure 4(E,C), Sup. Fig. 3 and 2B). Notably, the time to peak in the *ex vivo* studies were highly variable (ranging from a few seconds to minutes) and on average were more than 30 times longer than those seen after intravenous glucose injection (4.4 ± 0.5 sec *in vivo* and 140 ± 30 sec *ex vivo*, Figure 4(F)).

L-glutamine and palmitic acid also stimulate $[Ca^{2+}]_i$ influx in zebrafish pancreatic islet

In mammalian β-cells, excitation occurs not only in response to glucose but also to various other stimuli. [46–49] To test whether amino acids and free fatty acids contribute to $[Ca^{2+}]_i$ signalling of zebrafish pancreatic islets, perfusion experiments with L-glutamine and palmitic acid on extracted islets were carried out. Whole islets extracted from 5 dpf zebrafish larvae showed increase in GCaMP6s FIU/FIU baseline intensity when 20 mM L-glutamine or 1 mM palmitic acid alone and no glucose was applied in the perfusion system (Figure 5(A,B)). To confirm that the responses were specific to the nutrients and were not due to osmotic stress, we performed perfusion experiments with 20 mM sucrose on the extracted pancreatic islet; no significant increase in GCaMP6s
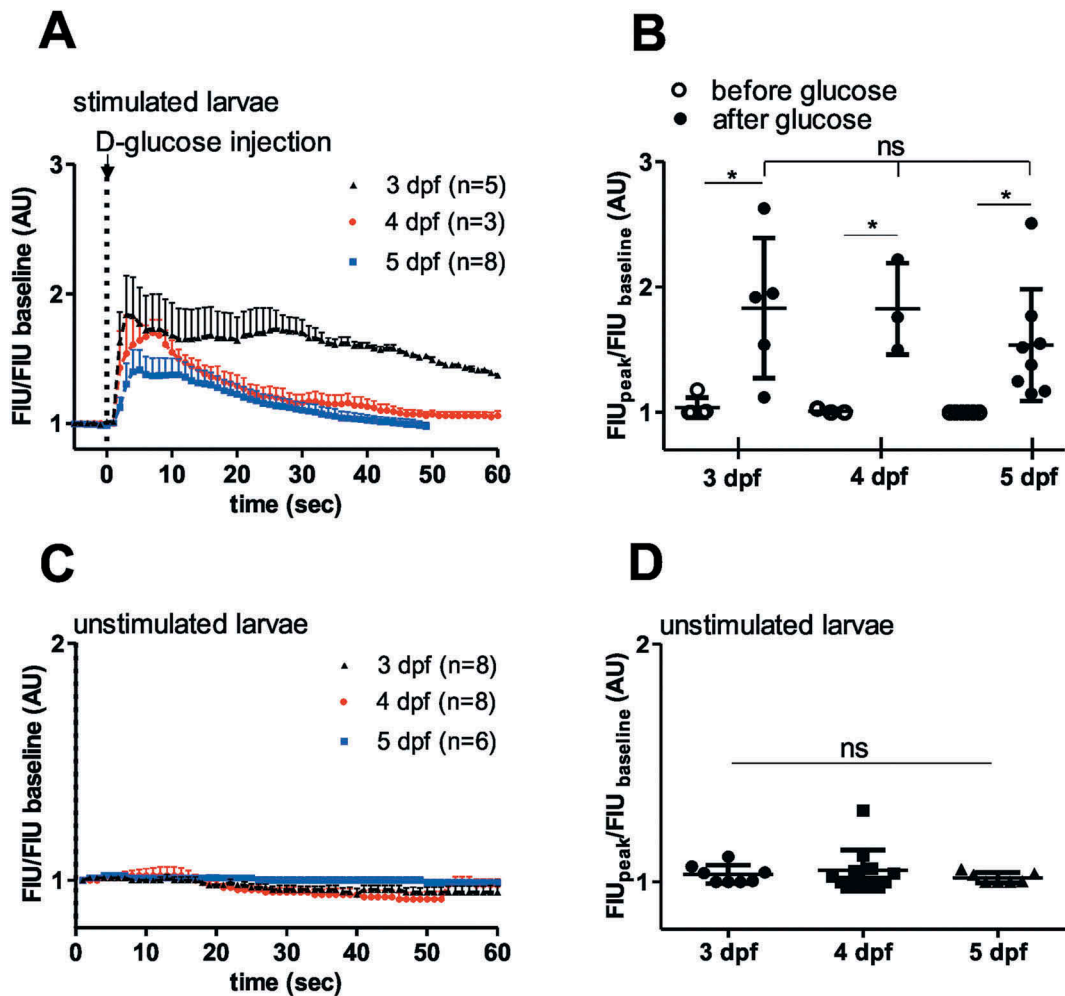
Figure 3. Similar *in vivo* glucose responses in 3 dpf, 4 dpf and 5 dpf zebrafish larvae.

(A) Quantitation GCaMP6 signal intensity show rapid fluorescence signal alteration after intravenous injection of D-glucose (>10 mM final concentration) in 3, 4 and 5 dpf larvae (n = 5, 3 and 8 larvae, respectively), **(C)** and no or little alteration in unstimulated larvae (n = 8, 8 and 6 larvae, respectively). FIU intensities for the whole islet were determined using Image-J and normalized to the FIU baseline (intensity measured in the first time point) **(B)** Peak FIU intensities (FIU$_{peak}$) of the whole islets before and after glucose injection (normalized to baseline FIU intensity measured in the first time point) (curves shown in (A) at different developmental stages (3, 4 and 5 dpf) (n = 5, 3 and 8 larvae, respectively). **(D)** Peak FIU intensities (FIU$_{peak}$) of the whole islets in unstimulated larvae (normalized to baseline FIU intensity measured in the first time point) (curves shown in (C)) at different developmental stages (3, 4 and 5 dpf) (n = 8, 8 and 6 larvae, respectively). FIU = Fluorescence Intensity Units (AU, Arbitrary Units). Data are shown as mean values ±s.d., *p < 0.05 in one-way ANOVA, Tukey's Multiple Comparison test to compare the glucose-injected groups (between 3, 4 and 5 dpf old larvae after glucose) in (B) and the unstimulated larvae in (D), and two-tailed, paired t-test was done to compare before and after glucose groups in (B).

fluorescence intensity was observed. In all cases, islets were excitable, as revealed by the change in fluorescence upon 30 mM KCl stimulation (Figure 5(C)). Again, Ca^{2+} fluctuations occurred asynchronously across the whole islet in all *ex vivo* conditions, indicating that β-cells were not coupled with one other (Figure 5(A,B), right panels). These results revealed that short-term exposure to L-glutamine alone or to palmitic acid, without glucose, stimulates [Ca^{2+}]$_i$ influx in embryonic zebrafish pancreatic islets.

Ca$_v$1.2/isl^{m458} mutant zebrafish are hyperglycemic

Next we used the ins:lynGCaMP6s reporter to assess β-cell specific defects in L-type calcium channel mutant zebrafish embryos. Currently, the
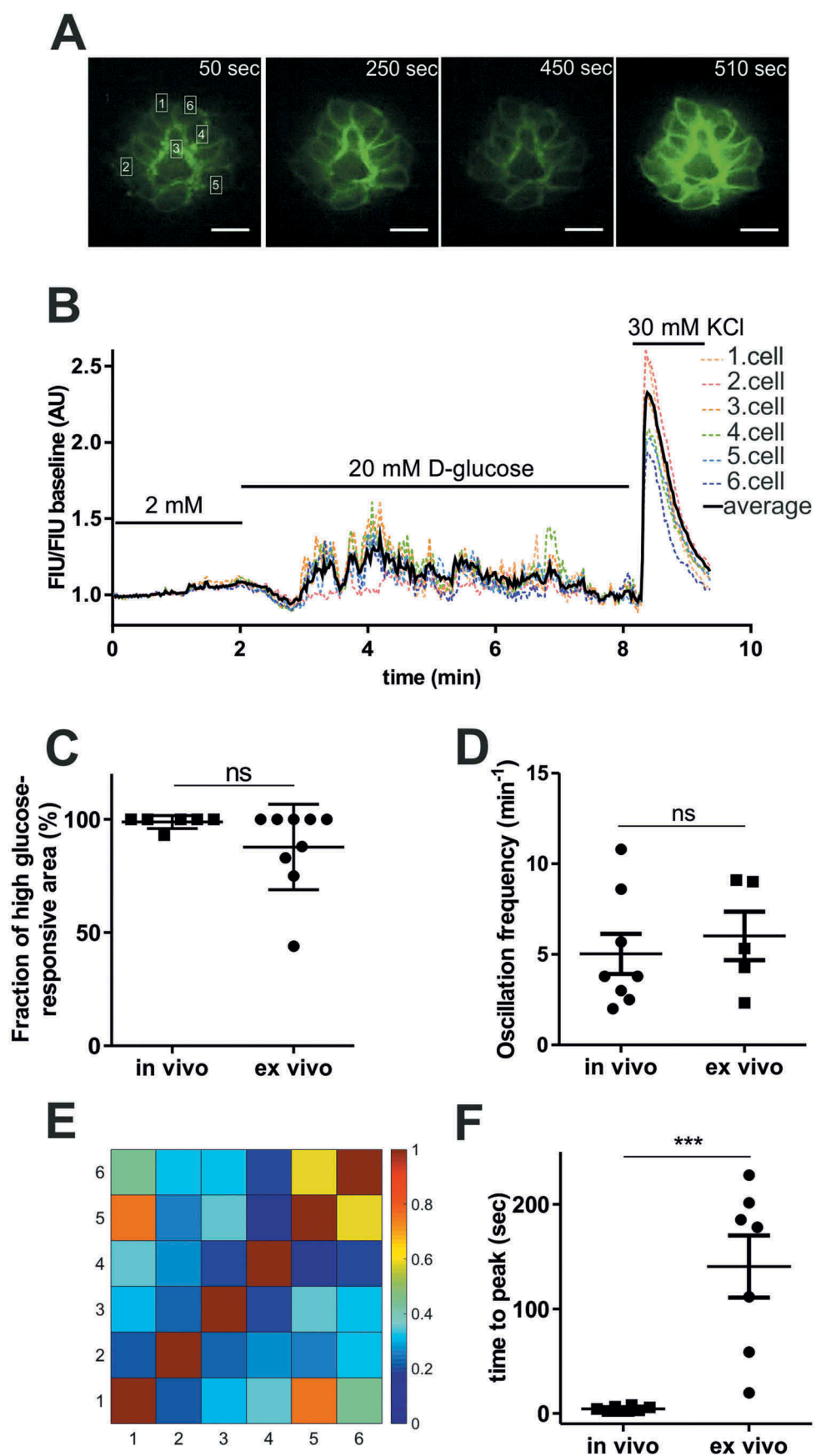
Figure 4. Comparison of *ex vivo* and *in vivo* glucose responsiveness.
(A) Fluorescence image series of isolated pancreatic islet showing GCaMP6 signal alteration at the indicated time-points shown in (B) applying 2 mM, 20 mM glucose and 30 mM KCl. Single β-cell is defined as ˜3 × 5 μm white rectangular selection drawn around one

genetic roles of $Ca_V1.2$ and $Ca_V1.3$ in glucose homeostasis are not well defined. Physiological studies indicate that $Ca_V1.2$ and $Ca_V1.3$ are key regulators of mammalian glucose-induced insulin secretion (for a review, see ref.[43]), but corresponding mouse knockout models displayed only minor effects on insulin secretion and glucose homeostasis, perhaps due to compensation by other channels. In particular, it was found that $Ca_V1.2$ in β-cells is required for proper first-phase glucose-induced insulin secretion, and that $Ca_V1.3$ may modulate second-phase secretion, each of which is significant for normal glucose tolerance.[40,43] The zebrafish has three $Ca_V1.2$ and $Ca_V1.3$ encoding gene orthologues, of which two – cacna1c (encoding $Ca_V1.2$) and cacna1da ($Ca_V1.3a$) – show expression in the developing pancreatic islet.[50–52] The third gene cacna1db ($Ca_V1.3b$) is exclusively expressed in the central nervous system.[51] To test cell type specific expression of $Ca_V1.2$ and $Ca_V1.3a$, we performed whole mount stains in different endocrine GFP-reporter stains (Sup. Fig. 4). We found that $Ca_V1.2$ and $Ca_V1.3a$ are expressed in all hormone-positive pancreatic cells of embryos older than one day (Sup. Fig. 4.). To determine requirements of these genes in glucose homeostasis, we took advantage of previously described mutants for $Ca_V1.2$ (isl, isl[m485], island beat)[50,53] and $Ca_V1.3a$ (gem, gem[tc323d], gemini).-[54,55] Both mutant alleles carry premature stop codons that result in the expression of truncated (and most likely inactive) proteins. Measurements

of free glucose in control and mutant embryos showed elevated glucose levels in 4–5 dpf $Ca_V1.2/$ isl[m458] (Figure 6(A) and Sup. Fig. 5) but normal glucose levels in 5 dpf $Ca_V1.3a/gem$[tc323d] mutants (Sup. Fig. 6). These data suggest impaired β-cell functionality in the $Ca_V1.2/isl$[m458] mutant fish.

To test whether $Ca_V1.2/isl$[m458] mutants affect β-cell specific $[Ca^{2+}]_i$ dynamics, the mutation was crossed into the ins:lynGCaMP6s background. In vivo fluorescence recordings of untreated 5 dpf transgenic larvae showed significantly higher basal islet $[Ca^{2+}]_i$ dynamics in mutants than control animals (Figure 6(C), Sup. Video 3 and 4). Hyperglycemia in these animals raised the possibility that non-islet effects could underlie the increased $[Ca^{2+}]_i$ dynamics in the $Ca_V1.2/isl$[m458] mutants. To eliminate non-islet effects, we performed ex vivo recordings of isolated mutant and control islets. Importantly, increased $[Ca^{2+}]_i$ dynamics in mutants were maintained in isolated islets and appeared to be glucose independent. In particular, we found that in mutant islets the change from 2 mM to 20 mM glucose had no significant effect on the peak frequency (2 mM: 0.6 ± 0.3 and 2.6 ± 0.7 peaks/min; 20 mM: 6.0 ± 1.0 and 1.8 ± 0.5, control and mutant, respectively) (Figure 6(C)), or on the integrated signal intensity (2 mM: 0.018 ± 0.004 and 0.065 ± 0.008 AUC; 20 mM: 0.057 ± 0.013 and 0.074 ± 0.011, control and mutant, respectively) (Figure 6(D) and Sup. Fig 7A), while in control islets these parameters were significantly increased

---

piece of the GCamP6s-expressing membrane located between two individual β-cells. Scale bar = 10 μm. **(B)** Single cell GCaMP6s fluorescence traces for isolated islet from wild-type zebrafish larvae (5 dpf) after applying 2 mM, 20 mM glucose followed by 30 mM KCl. FIU intensities for the single cells (n = 6 cells) were determined using Image-J, normalized to the FIU baseline (intensities measured in the first 2 min when 2 mM glucose was applied) and displayed as FIU/FIU baseline (AU) for single cells (coloured dotted line) and for the average of the singles cells in the islet (black line). **(C)** Quantification showing the percentage of β-cells that respond upon stimulation with 20 mM glucose, ex vivo and the percentage of glucose-responsive β-cell area after intravenous injection of >10 mM glucose in vivo. (n = 8 and 9 larvae were analyzed, in vivo and ex vivo, respectively) **(D)** Average oscillation frequencies of 4 selected β-cell areas of the pancreatic islet (n = 8 islets, in each islet 4 β-cell areas were manually selected based on the red RFP expression) after intravenous injection (~1–2 nl of 0.5 M glucose, >10 mM final concentration) of 5 dpf old zebrafish larvae (in vivo, imaged by epifluorescence microscope), and average oscillation frequencies of individual β-cells (n = 5 islets, in each islet >6 cells were analyzed) of the isolated pancreatic islets after 20 mM glucose stimulation (ex vivo, imaged by spinning disc microscope). Oscillation peaks were identified by PeakCaller, MATLAB on the FIU/FIU baseline traces of individual β-cells/areas (see Sup. Fig. 2A). The peak number was divided by the time duration until oscillation was observed (~30–60 sec, in vivo, ~150–300 sec, ex vivo) **(E)** Cross-correlation matrix (determined by PeakCaller, MATLAB) of the islet between individual cells shown in (A) and (B), with color key to the right of the matrix graph. Numbers on the x and y axes represent individual cells that are marked in (A) and (B). **(F)** Time to peak calculated from the time point when addition of the new glucose solution was finished in isolated islets, ex vivo (n = 7 islets, the addition took in average ~38 seconds), and when glucose was injected in living zebrafish larvae, in vivo (n = 8 islets from n = 8 larvae). Data are shown as mean values ±s.e.m., *p < 0.05 in unpaired, two-tailed t-test between ex vivo and in vivo groups in (C), (D) and (F). FIU = Fluorescence Intensity Units (AU, Arbitrary Units).
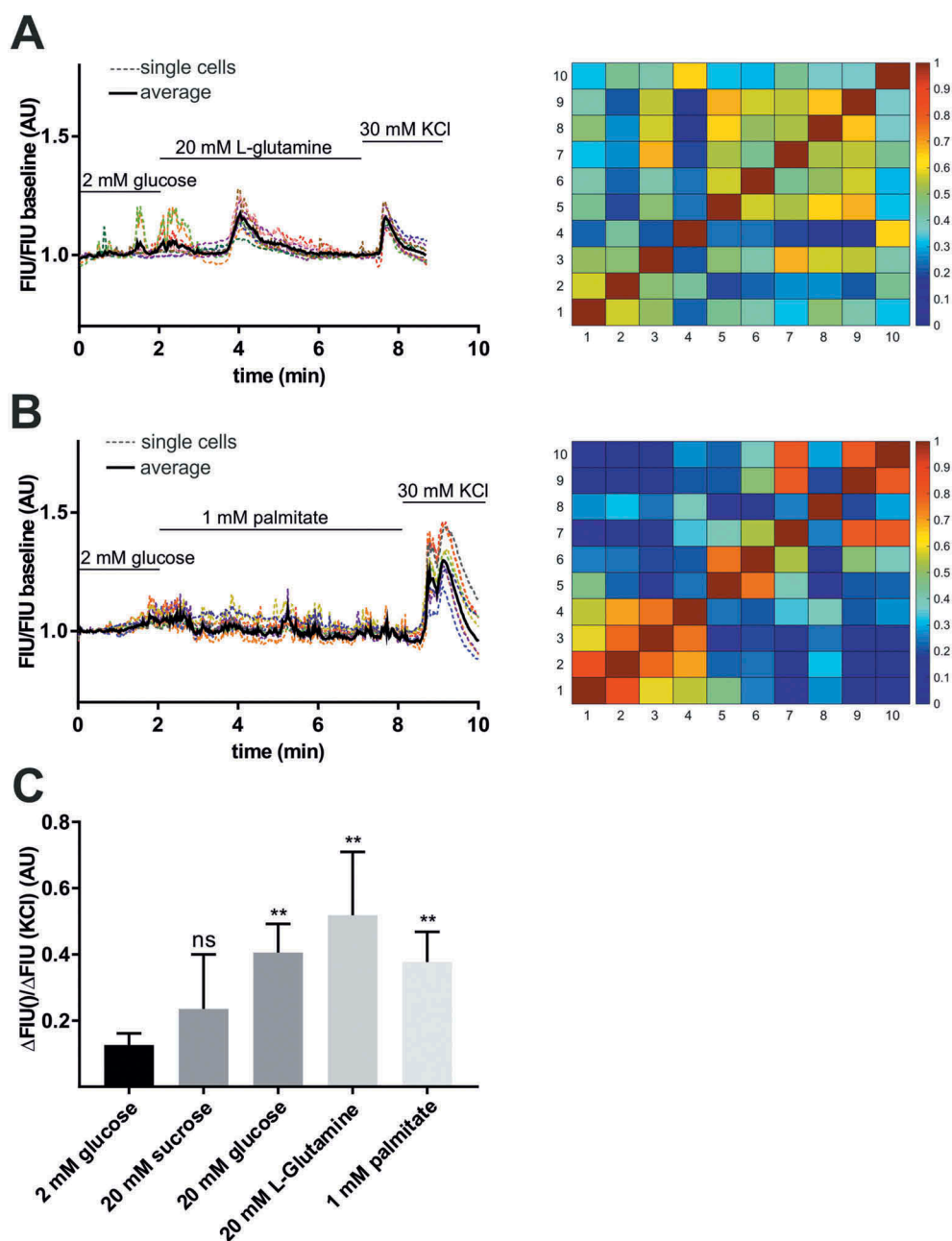
Figure 5. Stimulation of β-cell by L-glutamine and palmitic acid.

Representative single cell GCaMP6s fluorescence traces for isolated islet from wild-type zebrafish larvae (5 dpf) after applying 2 mM glucose followed by 20 mM L-glutamine **(A)**, and 1 mM palmitic acid **(B)** stimulation and 30 mM KCl. FIU intensities for the single cells (n = 10–10 cells) were determined using Image-J, normalized to the FIU baseline (intensities measured in the first 2 min when 2 mM glucose was applied) and displayed as FIU/FIU baseline (AU) for single cells (coloured dotted line) and for the average of the singles cells in the islet (black line). Cross-correlation matrices (determined by PeakCaller, MATLAB) of the islets between individual cells shown in (A) left panel and (B) left panel, with color key to the right of the matrix graph. Numbers on the x and y axes represent individual cells. Cross-correlation analysis was done on the section where L-glutamine/palmitate stimulation was applied (excluding KCl section). **(C)** Calcium responses to 20 mM L-glutamine and 1 mM palmitic acid when compared to 2 mM glucose. The changes in GCaMP6s fluorescence intensity in β-cells of wild-type pancreatic islets were averaged for the whole islet and the FIU peak intensity upon different nutrient stimulation was normalized to the FIU peak intensity upon KCl stimulation (n = 23, 7, 5, 4 and 7 islets were analyzed for 2 mM glucose, 20 mM glucose, 20 mM L-glutamine, 20 mM sucrose, and 1 mM palmitic acid stimulation, respectively) (in each islet at least n = 5–8 cells were analyzed and the FIU peak intensity was measured in the average FIU trace for the whole islet). Data are shown as mean values ±s.e.m., *p < 0.05 in unpaired t-test between 2 mM glucose and 20 mM sucrose, 20 mM L-glutamine, and 1 mM palmitic acid stimulation. FIU = Fluorescence Intensity Units (AU, Arbitrary Units).
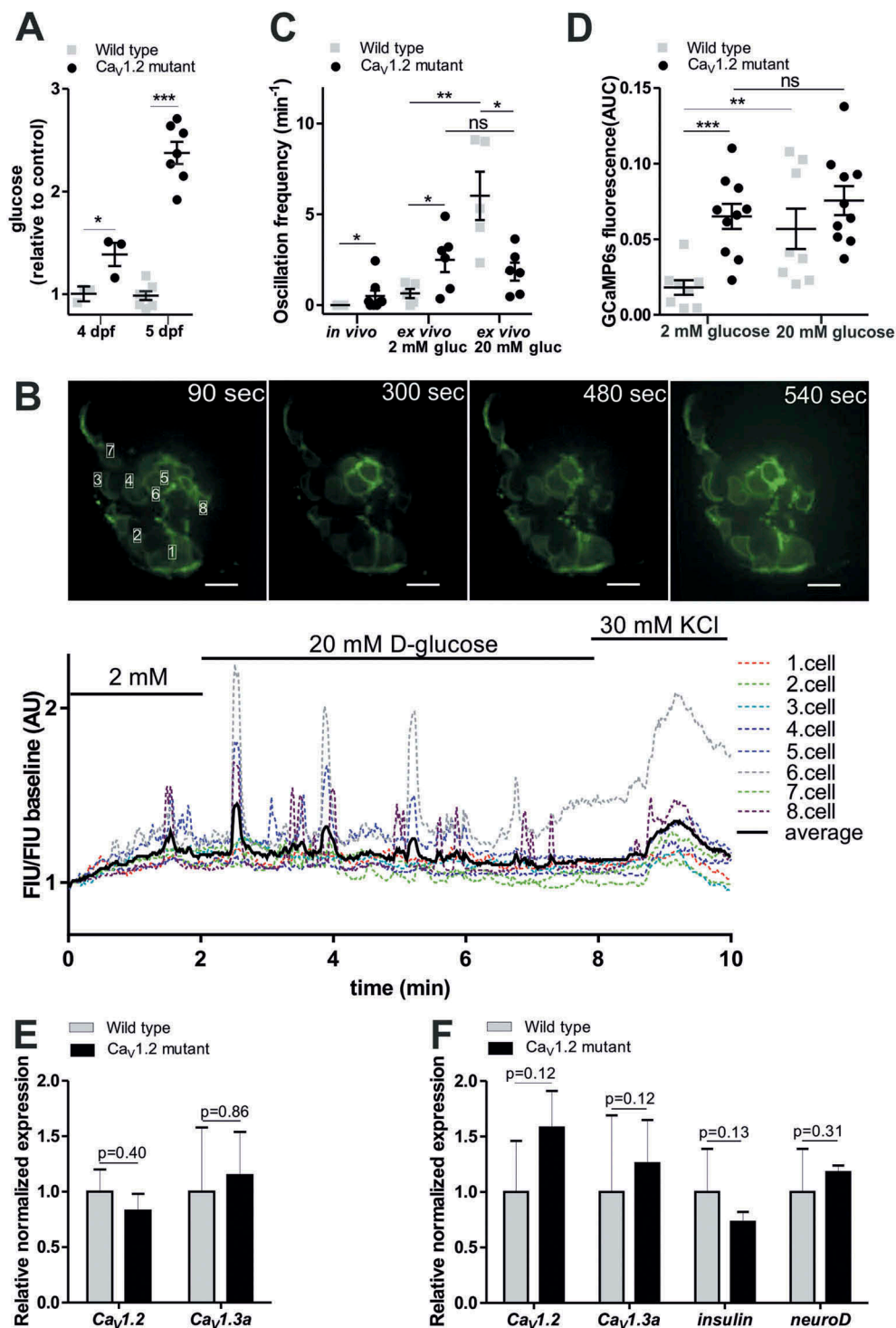
Figure 6. *Ex vivo* imaging of β-cells Ca^{2+}_i dynamics in $Ca_V1.2$ mutant zebrafish larvae.

(A) $Ca_V1.2/isl^{m458}$ mutant shows elevated whole larval glucose levels at 4 and 5 dpf. Glucose levels measured at 4 and 5 dpf whole larval extracts (pool of 10–10 larvae), normalized to the protein level measured by Nanodrop, and showed as relative to the average control value. (n = 4 and 8 biological replicates, respectively) (at 5 dpf, results combined from 2 independent experiments) (***p < 0.0001, two-tailed t-test). **(B)** Fluorescence image series of an isolated islet from 5 dpf old $Ca_V1.2$ mutant crossed with ins: lynGCaMP6s larva (upper panel). Quantitation of GCaMP signal intensity in the time series shown in the upper panel, indicating FIU/FIU baseline changes after 20 mM glucose as well as after 30 mM KCl stimulation (lower panel). **(C)** Quantification of GCaMP6s fluorescence intensity peaks determined by PeakCaller, MATLAB *in vivo*, without any stimulation (n = 6 wild type and 8 $Ca_V1.2$ mutant larva), and *ex vivo*, upon 2 and 20 mM glucose stimulation in wild-type and $Ca_V1.2$ mutant larva (n = 7–7 and 6–6 larvae, respectively), shown as oscillation frequency (min^{-1}) (peak number/cell number*minute). β-cell number was defined based on red nuclei RFP expression in one focal plane (4–10 cells per islet were analyzed) (**p < 0.005, two-tailed, nonparametric Mann-Whitney

by increasing glucose levels. Thus, there is a counterintuitive increase in $[Ca^{2+}]_i$ oscillations at basal glucose in the mutant islets. In mouse, $Ca_V1.3$ subunit knockout was found to be compensated by $Ca_V1.2$ upregulation.[42] To test whether upregulation of $Ca_V1.3a$ may account for the $Ca_V1.2/isl^{m458}$ mutant phenotype, we performed RT-qPCR (reverse transcriptase quantitative PCR) analyses. However, transcripts levels for $Ca_V1.2$ and $Ca_V1.3a$ in whole embryos (Figure 6(E)) and isolated islets (Figure 6(F)) showed no significant differences between controls and mutants. These data show that genetic loss of $Ca_V1.2$ results in glucose-independent hyperactivation of β-cells, and suggest that this activation is independent of cell-autonomous compensatory effects.

Discussion

We have successfully assessed $[Ca^{2+}]_i$ dynamics in β-cells of zebrafish pancreatic islets, both *in vivo* after injection of glucose and *ex vivo* using perfused isolated islet. We found that zebrafish β-cells are directly glucose-responsive, and that responsiveness is established early in embryonic development. These data are consistent with a conserved glucose sensing and stimulus-secretion coupling mechanism in fish and mammals. However, our analyses also showed that glucose-induced β-cell responses in perfused embryonic zebrafish islets are not well-synchronized, while β-cells in perfused mammalian islets show well-synchronized $[Ca^{2+}]_i$ oscillations throughout the whole islet.[56–58] In agreement with very recent *ex vivo* Ca^{2+} recordings of perfused juvenile zebrafish islet,[39] the data suggest that zebrafish islets are uncoupled, at least in the developing zebrafish.

We also evaluated different approaches for glucose administration in living zebrafish embryos. It is important to note that our *in vivo* imaging data, in contrast to the *ex vivo* data, did not allow analyses at single cell resolution. The combination of the deep tissue localization, the frequent presence of light absorbing pigment cells, and permanent slow tissue movements due to gut peristaltic movement prevented more detailed analyses. However, our data revealed that embryonic *in vivo* β-cell responses are immediate and synchronized when glucose is directly injected into the bloodstream, and that gradually increasing blood glucose levels result in delayed, non-synchronized $[Ca^{2+}]_i$ fluctuations, very similar to those found in glucose-stimulated perfused islets. Currently, we can only speculate about the mechanism underlying the synchronized responses after intravenous glucose injection. Possibly, the synchronicity is caused by a cell-autonomous but simultaneous response of all β-cells to the simultaneous prompt exposure to a high glucose challenge. Alternatively, synchronicity could be triggered by a currently undefined paracrine signal. In this context, the much faster $[Ca^{2+}]_i$ dynamics in living animals, as compared to isolated islets, could indicate the involvement of neuronal driven triggers. Consistent with this possibility, it was recently shown that the embryonic zebrafish islet is innervated at the relevant time points, and that a neurotransmitter, namely galanin expressed in these neurons, is involved in blood glucose regulation.[59,60] Notably, the delayed glucose response in the isolated zebrafish islets is similar to that seen in mammalian islets. While this delay is attributed to the time taken for glucose diffusion and metabolism,[61,62] it might be further affected by the cleavage of neural connection during the islet isolation procedure.[60] Measurements of real-time glucose response of pancreatic mouse islets by autofluorescence NAD(P)H signals also suggests that there might be differences in glucose metabolism after isolation.[63] However, the time to reach the initial GCaMP fluorescence peak after glucose injection in mice *in vivo* (~1–2 minutes) is still much

---

test) **(D)** Quantification of GCaMP6s fluorescence intensity *ex vivo* in wild-type and $Ca_V1.2$ mutant larvae shown as area under curve (AUC) upon 2 mM and 20 mM glucose stimulation normalized to the treatment duration (n = 9 and 10 larvae, respectively) (***p < 0.0005, two-tailed, unpaired t-test). **(E)** Relative normalized $Ca_V1.2$ and $Ca_V1.3a$ mRNA expression levels as determined by RT-qPCR (reverse transcriptase quantitative PCR) in 5 dpf old wild type and $Ca_V1.2$ mutant larvae (pools of 15 whole larvae) (n = 3 biological replicates, 2 technical replicates) **(F)** Relative normalized $Ca_V1.2$, $Ca_V1.3a$, *insulin* and *neuroD* mRNA expression levels determined by RT-qPCR in isolated pancreatic islets from 5 dpf old wild type and $Ca_V1.2$ mutant larva (pools of 15 islets) (n = 3 biological replicates, 2 technical replicates). Data are shown as mean values ±s.e.m (*p < 0.05, two-tailed t-test). FIU = Fluorescence Intensity Units (AU, Arbitrary Units).

slower than in our study in zebrafish (~5 sec).[35] Therefore, we also cannot exclude the possibility that the fast response in zebrafish is caused by bypassing glucose metabolism, with glucose activating $[Ca^{2+}]_i$ by other mechanisms, such as the swelling-sensing LRRC8 channels, for example, similar to mouse β-cells.[64] Detailed analyses is required to investigate the potential function of the LRRC8 proteins in zebrafish β-cells, but expression profiling of zebrafish islets cells suggests that the 5 *lrrc8* genes are differentially expressed between these cell types.[52,65]

Our finding that both palmitate and L-glutamine resulted in elevated $[Ca^{2+}]_i$ correlates with increased Ca^{2+} signalling and insulin secretion in mammalian islets exposed to free fatty acids and amino acids. However, and in contrast to mammalian islets, zebrafish embryonic islets did not require the simultaneous presence of glucose for elevated $[Ca^{2+}]_i$ signals.[47,66,67]

Our studies further reveal a novel central role of $Ca_V1.2$ in β-cell specific stimulus-secretion coupling in zebrafish. We find that genetic loss of $Ca_V1.2$ but not of $Ca_V1.3a$, results in elevated glucose level during development. Further, we show that β-cells in $Ca_V1.2/isl^{m458}$ mutant zebrafish display increased basal $[Ca^{2+}]_i$ and a complete loss of glucose-responsiveness. Future studies will be required to unravel the underlying mechanism of the increased basal activity of the $Ca_V1.2$ truncated β-cells. The counterintuitive increase in $[Ca^{2+}]_i$ oscillations at basal glucose in the mutant cells could be caused by an overcompensation of other VDCCs, as was seen in $Ca_V1.3$ knockout mice.[42] While our qPCR analyses revealed no evidence for up-regulation of $Ca_V1.2$ and $Ca_V1.3a$, this does not exclude the possibility of dysregulation of other Ca^{2+} channels (N-, P/Q-type), that might be expressed and functional in the zebrafish islet.[52] Importantly, our studies also suggest that β-cell specific $Ca_V1.2$ functions might be very different in zebrafish and mice. Notably, $Ca_V1.2$ mutant mice are not viable and therefore comparable embryonic β-cell defects have not been determined in the mouse mutants.[68] However, β-cell specific loss of $Ca_V1.2$ has only moderate effects on $[Ca^{2+}]_i$ handling and glucose responsiveness in mice, despite significantly reduced Ca_V currents and

inhibition of first-phase insulin secretion.[40] The expression of $Ca_V1.2$ not only in β-cells but rather in all pancreatic endocrine cells leaves other possibilities for non-cell autonomous β-cell defects due to paracrine effects such as dysfunctional α- or δ-cells. A disturbed intra-islet communication (for a review see ref.[69]) could explain why β-cell phenotypes in $Ca_V1.2/isl^{m458}$ mutants appear to be completely different from those seen in β-cell specific $Ca_V1.2$ knock-out mice.

Our demonstration of glucose-dependence of $[Ca^{2+}]_i$ provides support for zebrafish as an appropriate model to study stimulus-secretion coupling in the pancreas, both for fundamental understanding of secretion control, and for development of novel approaches to β-cell related diseases. However, in defining distinct consequences of manipulation of the voltage-gated L-type Ca^{2+} channel, our work also highlights the need to determine underlying differences between mammalian and zebrafish β-cell physiology to better understand this framework for applying zebrafish as a diabetes model.

Materials and methods

Zebrafish breeding and maintenance

Zebrafish (*Danio rerio*) were maintained according to standard protocols.[70] Developing embryos were staged by hours post fertilization (hpf) when incubated at 28°C.[71] All procedures were approved by the Austrian Bundesministerium für Wissenchaft und Forschung (GZ BMWFW-66.008/0004-WF/II/3b/2014).

Construction of Tg[ins:lynGCaMP6s,ins:H2B:RFP]

The lyn membrane tag sequence was PCR-amplified from pcDNA8D3cpv (Addgene plasmid #36323; Primer1: 5′TGGGATCCCCACCATGGGCTGCATCA-3′; Primer 2: 5′-TCTCTAGACCGGTATCGGGTGGATCGATTCTCAGTTTGGGTGGGGTCTTCATGTCCACGC-3′) and ligated into the pME vector using the BamHI and XbaI sites. Subsequently, the GCaMP6s sequence from Tol2 HuC GCaMP6s vector were added using

Age1 sites for ligation. The final construct was assembled by 4-fragment Gateway cloning (LR Clonase II Enzyme mix; Invitrogen, 11–791-100) using pDestTol2CG2 ins:H2B-RFP (Addgene plasmid), p5E insulin promoter, p3E polyA and the pME lynGCaMP6s plasmids.

Immunohistochemistry

Immunostaining of whole embryos or larvae was performed as previously described.[72] Larvae were collected at 5 dpf, and fixed for 2 hours at room temperature in 4% PFA/1% DMSO in PBS, then washed 3 × 5 minutes with 1 × PBS/0.1% Tween. Zebrafish embryos were incubated for one hour in blocking solution (PBS/1%DMSO/1%BSA/1% Triton), then incubated overnight at 4°C with primary antibodies diluted in blocking solution. Afterwards, washing was conducted with PBS+0.2% Triton. Primary antibodies and dilutions were: guinea pig anti-insulin (1:200, Dako, A0564), rabbit anti-GFP (1:200, Torrey Pines Biolabs, NC9589665). Secondary antibodies (1:1000 dilution) were Alexa-conjugated (Invitrogen). Embryos were washed and then reblocked, and incubated in secondary antibody overnight at 4°C.

Whole-mount in situ hybridization (WISH)

WISH was performed as described previously.[73] Antisense probes were Digoxigenin (DIG RNA Labeling Mix, Roche, 11277073910) labelled and visualized with α-Digoxigenin-AP antibody (1:4000, Roche, 11093274910). The following probes were used:

$Ca_V1.2$: $Ca_V1.2$ Xba S: GGACAACTTTG ACTATTTAACACGG; $Ca_V1.2$_R: CTGTTCCC CCTACAAACTCG

$Ca_V1.3a$: $Ca_V1.3a$ 5′ S: CTGAAAGGAAAGA CCTCATCAAAGAG, Ca_V13a_R: ACCAGGTGC TATAAAGTGGTAAT

All antisense RNA probes were generated by linearization of the corresponding plasmids and transcription was performed using T3, T7 or SP6 RNA polymerase. The eGFP of transgenic animals was visualized by immunostaining after the *in situ* hybridisation. Primary antibody: anti-GFP rabbit (1:200, Abcam, ab6556); secondary antibody: Alexa Fluor 488 goat anti-rabbit (1:1000, Roche, A32731). Immunostainings were performed as described above.

In vivo *glucose injection and imaging*

Larvae (3, 4 and 5 dpf) for live imaging were anesthetized using cold-shock (embryos in egg water-containing dishes are set directly on ice) and immobilized by injection of ~10 nl of 1 mg/ml purified α-bungarotoxin (BTX, B137, Sigma-Aldrich, T9641) either to the yolk or to the gut. After 10–15 minutes, embryos were embedded in 1.2 % low melt agarose and imaged either on a Leica DM6000B microscope equipped with a SPOT-RT3 digital camera (Diagnostic Instruments, Inc., Sterling Heights, MI) (intravenous injection) or on a Zeiss Cell Observer SD using a 25X water immersion objective (brain, yolk, pericardium injection). Time lapse images were collected with 500 ms–1000 ms time intervals, 50–100 ms exposure for GCaMP6s, and 150 ms for RFP, 2 × 2 binning. For adjusting the needle (GB120F-10, 69 × 1,20 × 100 mm with filament, Science Products GmbH) into the dorsal aorta, or into the hindbrain ventricle, yolk and pericardium, 5X or 10X dry objectives, and for intravenous injection of ~1–2 nl of 0.5 M glucose (Carl Roth GmBH) (final concentration of ~10–20 mM, assuming the blood volume of zebrafish embryo is 60 nl) (79) in combination with 1.25% Rhodamine B isothiocyanate-Dextran (R9379, Sigma-Aldrich) to confirm intravenous injection, 40X water objective was used (Sup.Video 1). *In vivo* imaging of hindbrain ventricle, yolk, pericardium glucose injection (~9 nl of 1 M glucose in combination with 1.25% Rhodamine B isothiocyanate-Dextran, final concentration of ~30 mM, assuming the total volume of a 5 dpf old larva is 300 nl),[74] unstimulated larvae and $Ca_V1.2$/isl mutants crossed with ins:lynGCaMP6s was carried out with a Zeiss Cell Observer SD spinning disc microscope using a 25X water immersion objective.

Larvae islet isolation

Zebrafish embryos at 5 dpf were euthanized using cold-shock, rolled onto their left sides and, using 26 G sterile hypodermic-needles, yolk and visceral organs were removed by applying gentle pressure using needles until fully separated. The islets were identified and confirmed by either GCaMP6s green fluorescence or RFP red fluorescence. Not all of the islet surrounding tissue was removed in order to avoid the collapse of the islet. Freshly dissected islets were transferred by glass pipette to RPMI (ThermoFisher 11875–093) supplemented with 1 mM HEPES, antibiotic solution (Sigma A5955, 10 mll−1 solution), 10% fetal bovine serum and diluted with glucose-free RPMI to final glucose concentration of 6.67 mM (zebrafish islet media) in a 12-wells culture plate. Islets were incubated at 28°C for 1.5–2 hours before imaging.

Glucose level measurement

Glucose levels in whole larvae were measured using Glucose Assay Kit (BioVision, K606-100) as previously described.[75] In brief, pools of 10 whole larvae were collected in 200 μl cold PBS, and lysed by glass bead (0.5 mm) homogenization in Precellys24 bead homogenizer (one cycle of 20 s at 5000 rpm) (Peqlab). After centrifugation (10, 000 rpm for 30 s at 4°C), supernatants were transferred into fresh tubes, and glucose assay was carried out according to manufacturer's recommendation. In all experiments, at least 3 biological replicates (10 whole larvae), and 2 technical replicates were measured.

Ex vivo imaging

Islets from ins:lynGCaMP6s were placed into glass-bottomed culture plates containing 2 mM glucose solution (2 mM glucose in KRBH salt solution: 114 mM NaCl, 4.7 mM KCl, 1.16 mM MgSO$_4$ heptahydrate, 1.2 mM KH$_2$PO$_4$, 2.5 mM CaCl$_2$ dihydrate, 5 mM NaHCO$_3$, 20 mM HEPES and 0.1 g/100 ml BSA) with agarose gel wells. Islets were imaged on a Zeiss Cell Observer SD using a 40X water immersion objective (time lapse with 500 ms-1 s time interval, 50 ms

exposure for GCaMP6s) while indicated solutions were changed using a handmade perfusion system (5 ml syringes connected to plastic tubes through 26 G needles). Salts and glucose were purchased from either Roth GmbH or AppliChem GmbH. Solutions containing 2 mM and 20 mM glucose, 20 mM L-glutamine (Thermo Fischer, 25030081), 1 mM palmitic acid (sodium salt, 98%, Thermo Fischer, 416700050) and 30 mM KCl were used.

Image analysis

Visiview software (Visitron Systems, Puchheim, Germany) (for in vivo intravenous glucose injection experiments) and ZEN software (for ex vivo experiments and in vivo brain, yolk, pericardium injection) were used to capture time lapses, and fluorescence images were processed using ImageJ (Fiji) ROI Analyzer.[76] StackReg plugin in the ImageJ/Fiji was used for the recursive alignment of time series, as previously described.[77] The ROI manager in ImageJ/Fiji was used to manually draw either rectangular selection (~3 × 5 μm) around one piece of the GCaMP6s-expressing membranes located between two individual β-cells (referred as single β-cell, in ex vivo experiments done by Zeiss spinning disc microscopy), or polygon selections around the whole islet or 4 non-overlapping single-cell sized β-cell areas per islet that were defined based on red nuclei RFP expression (called as β-cell area) (in vivo experiments done by Leica epifluorescence microscopy) to measure the mean GCaMP6s fluorescence intensity (FIU) for each time frame. The mean GCaMP6s FIU per β-cell/β-cell area or per islet was normalized to the baseline (which is calculated as the mean intensity during incubation in 2 mM glucose for ex vivo experiments, and as the intensity in the first time point for in vivo experiments) and displayed as FIU/FIU baseline trace (Arbitrary Unit, AU) over time (sec or min). To correct for fluorescence decay due to photo bleaching, non-linear regression analysis (2 phase exponential decay, without weight data points and fixing of parameters) was carried out using GraphPad Prism version 5.00 for Windows (GraphPad Software, La Jolla, California USA, www.graphpad.com). Total β-cell [Ca^{2+}]$_i$ dynamics (ex vivo) was quantified by two different methods, either by calculating the area

under the curve (AUC) as described previously,[35] or for quantitative curves in Figure 5(C) and Sup. Fig. 7, the glucose and other nutrient (sucrose, L-glutamine, palmitic acid) responses are shown normalized to the change in fluorescence in response to KCl (showing maximum islet depolarization), because the maximum excitability of an islet or β-cell can vary, and the intensity of the islet's fluorescence can also vary. For AUC analysis, we calculated the average of the single FIU/FIU baseline traces for 2 min before stimulation (basal $[Ca^{2+}]_i$ dynamics), and 6 min after 20 mM glucose stimulation (stimulated $[Ca^{2+}]_i$ dynamics), and normalized to the treatment duration (Figure 6(D)). For calculating the fraction of high glucose-responsive area (Figure 4(C)), the Ca^{2+} influx response was defined as positive when the normalized GCaMP6s FIU within the selected β-cell area (*in vivo*) or single β-cell (*ex vivo*) showed >7% increase in comparison to the time point before glucose injection or 20 mM glucose stimulation, and this increase in fluorescence intensity was higher than the peak fluorescence intensity at baseline. In all *ex vivo* experiments, β-cells that failed to show fluorescence increase (>7% compared to time point before stimulation) upon KCl stimulation were excluded from quantification. Cross-correlation analysis (Fig. 4(E), 5(A,B), Sup. Fig. 2B, 3) and identification of the peak numbers for oscillation frequencies (Figures 4 (D) and 6(C)) on the FIU/FIU baseline traces of individual β-cells/areas were done by PeakCaller in MATLAB[78] (required rise: 1%, required fall: 3%, max. lookback: 5 pts, max. lookahead: 5 pts) Cross-correlation analysis was done on the section where glucose stimulation was applied (excluding KCl section). Oscillation frequencies (min^{-1}) are average peak number per minute of selected β-cells (>6 cells, *ex vivo*) or β-cell areas (4 non-overlapping single-cell sized selected region based on RFP red expression, *in vivo*) normalized to the time duration until oscillation was observed in the time series (˜30–60 sec, *in vivo*, ˜150–300 sec, *ex vivo*).

qPCR

Total RNA was prepared from dissected islets of 5 dpf old zebrafish larvae (pool of 15 islets) and from whole zebrafish larvae (pool of 15 larvae) using Trizol (Ambion), cDNA was prepared using the First Strand cDNA synthesis kit (Thermo Scientific).

qPCR was performed in a CFX Connect Real-Time System (BioRad) using the HOT Fire-Pol EvaGreen qPCR Mic Plus (Solis BioDyne). Data shown is the average of 3 biological replicates, presented as gene expression level relative to controls, after normalization to the housekeeping gene *ef1alpha*. PCR primer pairs for $Ca_V1.2$ (5′ to 3′): TCTTCA GGTGTGCGACAGGA (F), CTTCTCACAAGGG CGGTTTG (R), $Ca_V1.3a$: CCTCAGGCTGT GCTTCTGCT (F), CACAGCTTGCCTGGCATA CA (R), *insulin*: GCCCAACAGGCTTCTTCTAC AAC (F), GCAGATTTAGGAGGAAGGAAACCC (R), *neuroD*: CTTTCAACACACCCTAGAGTTCC G (F), GCATCATGCTTTCCTCGCTGTATG (R), *ef1alpha*: TCTCTACCTACCCTCCTCTTGGTC (F), TTGGTCTTGGCAGCCTTCTGTG (R).

Statistics

Graphical and statistical analyses were performed using GraphPad Prism version 5.00 for Windows, GraphPad Software, La Jolla, California USA, www. graphpad.com. Significance was tested using two-tailed distribution and either t-test or ONE-way ANOVA analysis with p < 0.05 considered significant. Data presented are generally representative of at least three independent experiments (except as indicated). Error bars represent standard error (s.e.m) (except as indicated).

Disclosure of potential conflicts of interest

No potential conflicts of interest were disclosed.

ORCID

Reka Lorincz http://orcid.org/0000-0002-9077-3300
Christopher H. Emfinger http://orcid.org/0000-0002-9130-4194
Andrea Walcher http://orcid.org/0000-0001-6624-4284
Michael Giolai http://orcid.org/0000-0003-4166-8202
Maria S. Remedi http://orcid.org/0000-0003-2048-472X
Colin G. Nichols http://orcid.org/0000-0002-4929-2134
Dirk Meyer http://orcid.org/0000-0002-4020-4484

References

1. Krishnan K, Ma Z, Björklund A, Islam MS. Calcium signaling in a genetically engineered human pancreatic β-cell line. Pancreas. 2015;44(5):773–777. doi:10.1097/MPA.0000000000000318.

2. Almaça J, Liang T, Gaisano HY, Nam HG, Berggren PO, Caicedo A. Spatial and temporal coordination of insulin granule exocytosis in intact human pancreatic islets. Diabetologia. 2015;58(12):2810–2818. doi:10.1007/s00125-015-3747-9.

3. Dolenšek J, Špelič D, Klemen MS, Žalik B, Gosak M, Rupnik M, Stožer A. Membrane potential and calcium dynamics in beta cells from mouse pancreas tissue slices: theory, experimentation, and analysis. Sensors (Switzerland). 2015;15(11):27393–27419. doi:10.3390/s151127393.

4. Kenty JHR, Melton DA. Testing pancreatic islet function at the single cell level by calcium influx with associated marker expression. PLoS One. 2015;10(4):1–17. doi:10.1371/journal.pone.0122044.

5. Stožer A, Dolenšek J, Rupnik MS. Glucose-stimulated calcium dynamics in islets of langerhans in acute mouse pancreas tissue slices. PLoS One. 2013;8(1). doi:10.1371/journal.pone.0054638.

6. Leibiger IB, Berggren P-O. Intraocular in vivo imaging of pancreatic islet cell physiology/pathology. Mol Metab. 2017;6(9):1002–1009. doi:10.1016/j.molmet.2017.03.014.

7. Chandra R, Liddle RA. Recent advances in the regulation of pancreatic secretion. Curr Opin Gastroenterol. 2014. doi:10.1097/MOG.0000000000000099.

8. Seth A, Stemple DL, Barroso I. The emerging use of zebrafish to model metabolic disease. Dis Model Mech. 2013;6(5):1080–1088. doi:10.1242/dmm.011346.

9. Pan FC, Wright C. Pancreas organogenesis: from bud to plexus to gland. Dev Dyn. 2011;240(3):530–565. doi:10.1002/dvdy.22584.

10. Fernandez J, Valdeolmillos M. Synchronous glucose-dependent [Ca2+](i) oscillations in mouse pancreatic islets of Langerhans recorded in vivo. FEBS Lett. 2000;477(1–2):33–36. doi:10.1016/S0014-5793(00)01631-8.

11. Henquin JC. Triggering and amplifying pathways of regulation of insulin secretion by glucose71. Diabetes. 2000;49(11):1751–1760. doi:10.2337/diabetes.49.11.1751.

12. Heimberg H, De Vos A, Vandercammen A, Van Schaftingen E, Pipeleers D, Schuit F. Heterogeneity in glucose sensitivity among pancreatic beta-cells is correlated to differences in glucose phosphorylation rather than glucose transport. Embo J. 1993;12(7):2873–2879.

13. Moss LG, Caplan TV, Moss JB. Imaging beta cell regeneration and interactions with islet vasculature in transparent adult zebrafish. Zebrafish. 2013;10(2):249–257. doi:10.1089/zeb.2012.0813.

14. Andersson O, Adams BA, Yoo D, Ellis GC, Gut P, Anderson RM, German MS, Stainier DY. NIH Public Access. 2013;15(6):885–894. doi:10.1016/j.cmet.2012.04.018.Adenosine.

15. Argenton F, Zecchin E, Bortolussi M. Early appearance of pancreatic hormone-expressing cells in the zebrafish embryo. Mech Dev. 1999;87(1–2):217–221. doi:10.1016/S0925-4773(99)00151-3.

16. Zang L, Shimada Y, Nishimura N. Development of a novel zebrafish model for type 2 diabetes mellitus. Sci Rep. 2017;7(1). doi:10.1038/s41598-017-01432-w.

17. Marty N, Dallaporta M, Thorens B. Brain glucose sensing, counterregulation, and energy homeostasis. Physiology (Bethesda). 2007;22:241–251. doi:10.1152/physiol.00010.2007.

18. Polakof S, Mommsen TP, Soengas JL. Glucosensing and glucose homeostasis: from fish to mammals. Comp Biochem Physiol - B Biochem Mol Biol. 2011;160(4):123–149. doi:10.1016/j.cbpb.2011.07.006.

19. Röder PV, Wu B, Liu Y, Han W. Pancreatic regulation of glucose homeostasis. Exp Mol Med. 2016;48(3):e219. doi:10.1038/emm.2016.6.

20. Ro der PV, Wong X, Hong W, Han W. Molecular regulation of insulin granule biogenesis and exocytosis. Biochem J. 2016;473(18):2737–2756. doi:10.1042/BCJ20160291.

21. Gilon P, Henquin JC. Influence of membrane potential changes on cytoplasmic CA2+ concentration in an electrically excitable cell, the insulin-secreting pancreatic B-cell. J Biol Chem. 1992;267(29):20713–20720.

22. Eames SC, Philipson LH, Prince VE, Kinkel MD. Blood sugar measurement in zebrafish reveals dynamics of glucose homeostasis. Zebrafish. 2010;7(2):205–213. doi:10.1089/zeb.2009.0640.

23. Remedi MS, Emfinger C. Pancreatic β-cell identity in diabetes. Diabetes, Obes Metab. 2016 September;18:110–116. doi:10.1111/dom.12727.

24. Jurczyk A, Roy N, Bajwa R, Gut P, Lipson K, Yang C, Covassin L, Racki WJ, Rossini AA, Phillips N, et al. Dynamic glucoregulation and mammalian-like responses to metabolic and developmental disruption in zebrafish. Gen Comp Endocrinol. 2011;170(2):334–345. doi:10.1016/j.ygcen.2010.10.010.

25. Tseng Y, Chen R, Lee J, Liu S, Lee S, Hwang P. Specific expression and regulation of glucose transporters in zebrafish ionocytes. Am J Physiol-Reg I. 2009;297(2):275–290. doi:10.1152/ajpregu.00180.2009.

26. Marín-Juez R, Rovira M, Crespo D, van der Vaart M, Spaink HP, Planas JV. GLUT2-mediated glucose uptake

and availability are required for embryonic brain development in zebrafish. J Cereb Blood Flow Metab. 2015;35(1):74–85. doi:10.1038/jcbfm.2014.171.

27. Cohen M, Kitsberg D, Tsytkin S, Shulman M, Aroeti B, Nahmias Y. Live imaging of GLUT2 glucose-dependent trafficking and its inhibition in polarized epithelial cysts. Open Biol. 2014;4(7):140091. doi:10.1098/rsob.140091.

28. Emfinger CH, Welscher A, Yan Z, Wang Y, Conway H, Moss JB, Moss LG, Remedi MS, Nichols CG. Expression and function of ATP-dependent potassium channels in zebrafish islet β-cells. R Soc Open Sci. 2017;4(2):160808. doi:10.1098/rsos.160808.

29. Li M, Maddison LA, Page-McCaw P, Chen W. Overnutrition induces -cell differentiation through prolonged activation of -cells in zebrafish larvae. AJP Endocrinol Metab. 2014. doi:10.1152/ajpendo.00686.2013.

30. Pace CS, Price S. Electrical responses of pancreatic islet cells to secretory stimuli. Biochem Biophys Res Commun. 1972;46(4):1557–1563. doi:10.1016/0006-291X(72)90785-1.

31. Grynkiewicz G, Poenie M, Tsien RY. A new generation of Ca2+ indicators with greatly improved fluorescence properties. J Biol Chem. 1985;260(6):3440–3450.

32. Bootman MD, Rietdorf K, Collins T, Walker S, Sanderson M. Ca2+-sensitive fluorescent dyes and intracellular Ca2+ imaging. Cold Spring Harb Protoc. 2013;8(2):83–99. doi:10.1101/pdb.top066050.

33. Matveyenko AV, Butler PC. Relationship between β-cell mass and diabetes onset. Diabetes Obes Metab. 2008;10:23–31. doi:10.1111/j.1463-1326.2008.00939.x.

34. Gotthardt M, Eizirik DL, Cnop M, Brom M. Beta cell imaging - a key tool in optimized diabetes prevention and treatment. Trends Endocrinol Metab. 2014;25(8):375–377. doi:10.1016/j.tem.2014.02.002.

35. Chen C, Chmelova H, Cohrs CM, Chouinard JA, Jahn SR, Stertmann J, Uphues I, Speier S. Alterations in β-cell calcium dynamics and efficacy outweigh islet mass adaptation in compensation of insulin resistance and prediabetes onset. Diabetes. 2016;65(9):2676–2685. doi:10.2337/db15-1718.

36. Barros TP, Alderton WK, Reynolds HM, Roach AG, Berghmans S. Zebrafish: an emerging technology for in vivo pharmacological assessment to identify potential safety liabilities in early drug discovery. Br J Pharmacol. 2008;154(7):1400–1413. doi:10.1038/bjp.2008.249.

37. Henke K, Bowen ME, Harris MP. Perspectives for identification of mutations in the zebrafish: making use of next-generation sequencing technologies for forward genetic approaches. Methods. 2013;62(3):185–196. doi:10.1016/j.ymeth.2013.05.015.

38. Kamel M, Ninov N. Catching new targets in metabolic disease with a zebrafish. Curr Opin Pharmacol. 2017;37:41–50. doi:10.1016/j.coph.2017.08.007.

39. Singh SP, Janjuha S, Hartmann T, Kayisoglu Ö, Konantz J, Birke S, Murawala P, Alfar EA, Murata K, Eugster A, et al. Different developmental histories of beta-cells generate functional and proliferative heterogeneity during islet growth. Nat Commun. 2017;8(1). doi:10.1038/s41467-017-00461-3.

40. Schulla V, Renström E, Feil R, Feil S, Franklin I, Gjinovci A, Jing XJ, Laux D, Lundquist I, Magnuson MA, et al. Impaired insulin secretion and glucose tolerance in beta cell-selective Ca(v)1.2 Ca2+ channel null mice. Embo J. 2003;22(15): 3844–3854.doi:10.1093/emboj/cdg389.

41. U.K. Prospective Diabetes Study Group. Overview of 6 years' therapy of type II diabetes: a progressive disease. Diabetes. 1995;44:1249–1258. doi:10.2337/db06-0880.CHS.

42. Namkung Y, Skrypnyk N, Jeong MJ, Lee T, Lee MS, Kim HL, Chin H, Suh PG, Kim SS, Shin HS. Requirement for the L-type Ca(2+) channel alpha(1D) subunit in postnatal pancreatic beta cell generation. Jci. 2001;108(7):1015–1022. doi:10.1172/JCI13310.

43. Yang S-N, Berggren P-O. The role of voltage-gated calcium channels in pancreatic beta-cell physiology and pathophysiology. Endocr Rev. 2006;27(6):621–676. doi:10.1210/er.2005-0888.

44. Stolovich-Rain M, Enk J, Vikesa J, Nielsen FC, Saada A, Glaser B, Dor Y. weaning triggers a maturation step of pancreatic β cells. Dev Cell. 2015;32(5):535–545. doi:10.1016/j.devcel.2015.01.002.

45. Musson MC, Jepeal LI, Mabray PD, Zhdanova IV, Cardoso WV, Wolfe MM. Expression of glucose-dependent insulinotropic polypeptide in the zebrafish. Am J Physiol Regul Integr Comp Physiol. 2009;297: R1803–R1812. doi:10.1152/ajpregu.00288.2009.

46. Newsholme P, Brennan L, Bender K. Amino acid metabolism, β-cell function, and diabetes. Diabetes. 2006;55 (Suppl. 2). doi:10.2337/db06-S006.

47. Gravena C, Mathias PC, Ashcroft SJH. Acute effects of fatty acids on insulin secretion from rat and human islets of Langerhans. J Endocrinol. 2002;173(1):73–80. doi:10.1677/JOE.0.1730073.

48. Malaisse WJ, Best L, Kawazu S, Malaisse-Lagae F, Sener A. The stimulus-secretion coupling of glucose-induced insulin release: fuel metabolism in islets deprived of exogenous nutrient. Arch Biochem Biophys. 1983;224(1):102–110. doi:10.1016/0003-9861(83)90193-5.

49. Zhang Y, Louchami K, Carpentier YA, Malaisse WJ, Sener A. L-glutamine and palmitate catabolism in pancreatic islets from rats depleted in long-chain polyunsaturated ω3 fatty acids. Cell Biochem Funct. 2008;26(1):82–86. doi:10.1002/cbf.1403.

50. Rottbauer W, Baker K, Wo ZG, Mohideen MA, Cantiello HF, Fishman MC. Growth and function of the embryonic heart depend upon the cardiac- specific L-type calcium channel alpha1 subunit. Dev Cell. 2001;1(2):265–275.

51. Sidi S, Busch-Nentwich E, Friedrich R, Schoenberger U, Nicolson T. gemini encodes a zebrafish L-type calcium channel that localizes at sensory hair cell ribbon synapses. J Neurosci. 2004;24(17):4213–4223. doi:10.1523/JNEUROSCI.0223-04.2004.

52. Tarifeño-Saldivia E, Lavergne A, Bernard A, Padamata K, Bergemann D, Voz ML, Manfroid I, Peers B.

Transcriptome analysis of pancreatic cells across distant species highlights novel important regulator genes. BMC Biol. 2017;15(1):21. doi:10.1186/s12915-017-0362-x.

53. Stainier DY, Fouquet B, Chen JN, Warren KS, Weinstein BM, Meiler SE, Mohideen MA, Neuhauss SC, Solnica-Krezel L, Schier AF, et al. Mutations affecting the formation and function of the cardiovascular system in the zebrafish embryo. Development. 1996;123:285–292.

54. Granato M, van Eeden FJ, Schach U, Trowe T, Brand M, Furutani-Seiki M, Haffter P, Hammerschmidt M, Heisenberg CP, Jiang YJ, et al. Genes controlling and mediating locomotion behavior of the zebrafish embryo and larva. Development. 1996;123(1):399–413.

55. Nicolson T, Rüsch A, Friedrich RW, Granato M, Ruppersberg JP, Nüsslein-Volhard C. Genetic analysis of vertebrate sensory hair cell mechanosensation: the zebrafish circler mutants. Neuron. 1998;20(2):271–283. doi:10.1016/S0896-6273(00)80455-9.

56. Gylfe E, Grapengiesser E, Hellman B. Propagation of cytoplasmic Ca2+ oscillations in clusters of pancreatic β-cells exposed to glucose. Cell Calcium. 1991;12(2–3):229–240.

57. Martín F, Soria B. Glucose-induced [Ca2+]i oscillations in single human pancreatic islets. Cell Calcium. 1996;20 (5):409–414. doi:10.1016/S0143-4160(96)90003-2.

58. Jonkers FC, Jonas JC, Gilon P, Henquin JC. Influence of cell number on the characteristics and synchrony of Ca2+ oscillations in clusters of mouse pancreatic islet cells. J Physiol. 1999;520(Pt 3):839–849.

59. Podlasz P, Jakimiuk A, Chmielewska-Krzesinska M, Kasica N, Nowik N, Kaleczyc J. Galanin regulates blood glucose level in the zebrafish: a morphological and functional study. Histochem Cell Biol. 2016. doi:10.1007/s00418-015-1376-5.

60. Yang YHC, Kawakami K, Stainier DY. A new mode of pancreatic islet innervation revealed by live imaging in zebrafish. Elife. 2018;7:e34519. doi:10.7554/eLife.34519.

61. Yamada K, Nakata M, Horimoto N, Saito M, Matsuoka H, Inagaki N. Measurement of glucose uptake and intracellular calcium concentration in single, living pancreatic ??-cells. J Biol Chem. 2000;275(29):22278–22283. doi:10.1074/jbc.M908048199.

62. Kaminski MT, Lenzen S, Baltrusch S. Real-time analysis of intracellular glucose and calcium in pancreatic beta cells by fluorescence microscopy. Biochim Biophys Acta. 2012;1823(10):1697–1707. doi:10.1016/j.bbamcr.2012.06.022.

63. Li G, Wu B, Ward MG, Chong ACN, Mukherjee S, Chen S, Hao M. Multifunctional in vivo imaging of pancreatic islets during diabetes development. J Cell Sci. 2016;129(14). doi:10.1242/jcs.190843.

64. Kang C, Xie L, Gunasekar SK, Mishra A, Zhang Y, Pai S, Gao Y, Kumar A, Norris AW, Stephens SB, et al. SWELL1 is a glucose sensor regulating β-cell excitability and systemic glycaemia. Nat Commun. 2018;9(1). doi:10.1038/s41467-017-02664-0.

65. Yamada T, Wondergem R, Morrison R, Yin VP, Strange K. Leucine-rich repeat containing protein LRRC8A is essential for swelling-activated Cl – currents and embryonic development in zebrafish. Physiol Rep. 2016;4(19):e12940. doi:10.14814/phy2.12940.

66. Rorsman P, Braun M, Zhang Q. Regulation of calcium in pancreatic α- and β-cells in health and disease. Cell Calcium. 2012. doi:10.1016/j.ceca.2011.11.006.

67. Liu Z, Jeppesen PB, Gregersen S, Chen X, Hermansen K. Dose- and glucose-dependent effects of amino acids on insulin secretion from isolated mouse islets and clonal INS-1E beta-cells. Rev Diabet Stud. 2008;5 (4):232–244. doi:10.1900/RDS.2008.5.232.

68. Seisenberger C, Specht V, Welling A, Platzer J, Pfeifer A, Kühbandner S, Striessnig J, Klugbauer N, Feil R, Hofmann F. Functional embryonic cardiomyocytes after disruption of the L-type α1C (Cav1.2) calcium channel gene in the mouse. J Biol Chem. 2000. doi:10.1074/jbc.M006467200.

69. Brereton MF, Vergari E, Zhang Q, Clark A. Alpha-, delta- and PP-cells: are they the architectural cornerstones of islet structure and co-ordination? J Histochem Cytochem. 2015;63(8):575–591. doi:10.1369/0022155415583535.

70. Westerfield M. The zebrafish book. a guide for the laboratory use of zebrafish (Danio rerio). 5th ed.: Univ Oregon Press, Eugene; 2007.

71. Kimmel CB, Ballard WW, Kimmel SR, Ullmann B, Schilling TF. Stages of embryonic development of the zebrafish. Dev Dyn. 1995;203(3):253–310. doi:10.1002/aja.1002030302.

72. Kimmel RA, Dobler S, Schmitner N, Walsen T, Freudenblum J, Meyer D. Diabetic pdx1-mutant zebrafish show conserved responses to nutrient overload and anti-glycemic treatment. Sci Rep. 2015 August;5:14241. doi:10.1038/srep14241.

73. Thisse C, Thisse B. High-resolution in situ hybridization to whole-mount zebrafish embryos. Nat Protoc. 2008;3(1):59–69. doi:10.1038/nprot.2007.514.

74. Guo Y, Veneman WJ, Spaink HP, Verbeek FJ. Three-dimensional reconstruction and measurements of zebrafish larvae from high-throughput axial-view in vivo imaging. Biomed Opt Express. 2017;8(5):2611. doi:10.1364/BOE.8.002611.

75. Kimmel RA, Meyer D. Zebrafish pancreas as a model for development and disease. Elsevier Ltd; 2016. Vol. 134. doi:10.1016/bs.mcb.2016.02.009.

76. Schneider CA, Rasband WS, Eliceiri KW. NIH Image to ImageJ: 25 years of image analysis. Nat Methods. 2012;9(7):671–675. doi:10.1038/nmeth.2089.

77. Thévenaz P, Ruttimann UE, Unser M. A pyramid approach to subpixel registration based on intensity. IEEE Trans Image Process. 1998;7(1):27–41. doi:10.1109/83.650848.

78. Artimovich E, Jackson RK, Kilander MBC, Lin YC, Nestor MW. PeakCaller: an automated graphical interface for the quantification of intracellular calcium obtained by high-content screening. BMC Neurosci. 2017;18(1). doi:10.1186/s12868-017-0391-y.